Applied Catalysis B: Environmental 123–124 (2012) 391–397

Contents lists available at SciVerse ScienceDirect

Applied Catalysis B: Environmental

journal homepage: www.elsevier.com/locate/apcatb

Enhancement of photocatalytic activity of titania–titanate nanotubes by surface modification

Soonhyun Kim*, Minsun Kim, Sung-Ho Hwang, Sang Kyoo Lim

Division of Nano-Bio Technology, Daegu Gyeongbuk Institute of Science and Technology (DGIST), Daegu 711-873, Republic of Korea

ARTICLE INFO

Article history:
Received 12 March 2012
Received in revised form 4 May 2012
Accepted 6 May 2012
Available online 12 May 2012

Keywords:
Photocatalysis
Titanate nanotubes
Titania
Hydrothermal reaction
Surface modification

ABSTRACT

Hydrothermally prepared titanate nanotubes are known to be thermodynamically unstable and to be easily transformed to the titania phase by heat or acid treatment, which is accompanied by the destruction of the nanotube structures. Surface modification of titanate nanotubes is expected to retard the phase-transition reactions from titanate nanotubes to titania nanoparticles. In this study, we investigated the effects of surface modifications, such as fluorination or phosphation, on the phase-transition reactions of hydrothermally prepared titanate nanotubes under acidic conditions. After acid treatment, surface-modified titanate nanotubes maintained their nanotube structures, and spherical nanoparticles were partially formed in the titanate nanotubes. Unmodified titanate nanotubes, however, changed to elongated nanostructures and spherical nanoparticles. The surface modifications also strongly affected the crystalline phases and increased the BET surface area. The photocatalytic activities for methylene blue degradation and gaseous CH_3CHO oxidation were strongly enhanced by the surface modifications. These effects were attributed to the anatase crystalline phase and the high surface area. Therefore, these surface modifications are useful methods to improve the photocatalytic activities of titanate nanotubes.

1. Introduction

Nanostructured materials derived from TiO_2 have been extensively developed to have novel properties and improved performance in various applications. TiO_2-based nanotubes with a high specific surface area, ion-changeable ability, and photocatalytic ability have been considered for an extensive number of applications [1,2]. TiO_2-based nanotubes are synthesized by three different methods: (i) the assisted-template method [3], (ii) electrochemical anodic oxidation [4], and (iii) hydrothermal treatment [5,6]. Among these methods, hydrothermal treatment has received the most attention because of its cost-effectiveness and the fact that it provides a simple route to the synthesis of nanotubes. TiO_2-based nanotubes, more precisely titanate nanotubes, formed by hydrothermal treatment were first reported by Kasuga et al. [5]. Nanotubes from TiO_2 particles were formed by the scrolling mechanism of exfoliated TiO_2-derived nanosheets [6–9]. Under alkaline hydrothermal conditions, other morphologies of nanostructured titanates, including nanotubes, nanosheets, nanorods/nanowires, and nanoribbons/nanobelts, have also been observed. However, the crystalline structure and the detailed formation mechanisms of titanate nanotubes are still a topic of discussion [5,8–12].

The photocatalytic activities of hydrothermally synthesized titanates are lower than those of commercial TiO_2 nanoparticles despite their higher surface area. Therefore, many researchers have attempted to enhance their photocatalytic activities through the phase transition of titanate nanotubes to anatase crystallites via calcination [13–16], H_2O_2 treatment [17], or hydrothermal treatment [18–20]. However, the phase transition of nanotubes often results in the conversion of the nanotube structures into nanoparticles. Bavykin et al. have previously reported that titanate nanotubes have a metastable nature and are intermediate species during the transformation of titania to titanates [21]. Although hydrothermally prepared titanate nanotubes are metastable and their photocatalytic activities are quite low, nanotube structures are still attractive. Therefore, if the phase-transition reaction from titania to titanate or vice versa could be controlled, the development of titania–titanate nanotube structures with efficient photocatalytic activities might be possible.

In this study, we investigated the effects of surface modifications, such as fluorination [22–24] or phosphation [25], on the phase-transition reactions of hydrothermally prepared titanate nanotubes under acidic conditions. These surface modifications are expected to retard the phase transition from titanate nanotubes to titania nanoparticles. For the phase-transition reaction, the hydrothermally synthesized titanate nanotubes were reacted with acid at a moderate temperature, which is known as the acid-treatment reaction. The fluoride or phosphate ions were added to

* Corresponding author. Tel.: +82 53 785 3410; fax: +82 53 785 3439.
E-mail address: sh2358@dgist.ac.kr (S. Kim).

0926-3373/$ – see front matter © 2012 Elsevier B.V. All rights reserved.
http://dx.doi.org/10.1016/j.apcatb.2012.05.008

the solution during the acid-treatment reaction. The physicochemical properties of the surface modified samples and unmodified samples were subsequently compared, and their photocatalytic activities for both the degradation of aqueous methylene blue (MB) and the oxidation of gaseous CH_3CHO were examined.

2. Experimental

2.1. Preparation of titanate nanotubes

P25 was added to 200 ml of 10 M NaOH solution, and the mixture was hydrothermally reacted at 120 °C for 24 h under stirring. The precipitates were then washed with distilled water until the washing solution reached pH 7, and the precipitates were subsequently freeze dried. The obtained titanate powder was denoted as TiNT. For the acid treatment, the TiNT was added to 100 ml of 0.1 M HNO_3 solution, and the mixture was refluxed at 80 °C for 24 h. These precipitates were then washed with distilled water and freeze-dried. The acid-treated TiNT powder was denoted as TiNT–AT. For surface modification, the TiNT was added to 100 ml of 0.1 M HNO_3 with $NH_4H_2PO_4$ (AdP) or NaF. The concentrations of AdP or NaF in the mixed solutions were 0.1 M. The mixtures were refluxed at 80 °C for 24 h. The precipitates were then washed with distilled water and freeze dried. The obtained powders were denoted as TiNT–AT–AdP and TiNT–AT–NaF.

2.2. Characterization

Transmission electron micrographs were obtained on a high-resolution transmission electron microscope (HR-TEM, JEM-2200FS). X-ray diffraction (XRD) patterns were obtained with an X-ray diffractometer (Rigaku D/MAX-2500, 18 kV) using Cu-K_{a1} radiation. Diffuse-reflectance UV–visible absorption spectroscopy (DRS) of the powder samples was performed on a spectrophotometer (Varian Cary 100) equipped with a diffuse-reflectance accessory. Zeta potentials were measured using an electrophoretic light-scattering spectrophotometer (Zetasizer, Malvern). The Brunauer–Emmett–Teller (BET) surface areas were determined from nitrogen adsorption–desorption isotherms at 77 K (ASAP 2020, Micromeritics). The effective surface areas were estimated at a relative pressure (P/P_0) that ranged from 0.01 to 0.1. The oxidation states of Na, P, and F atoms were determined by X-ray photoelectron spectroscopy (XPS) (Kratos XSAM 800pci) using the Mg-K_α line (1253.6 eV) as the excitation source.

2.3. Photocatalytic activity measurements

The photocatalytic degradation of MB was determined in aqueous suspensions. Each photocatalyst powder was dispersed in distilled water at 0.5 g/l and sonicated for 30 s. The desired amount of MB stock solution was added to the suspension, the solution pH was adjusted with HCl or NaOH, and the suspension was stirred for 30 min in the dark for equilibrium adsorption of the substrate onto the photocatalyst surface. A 300 W Xe arc lamp (Oriel) was used as the light source. The light beam was passed through a 10 cm IR water filter and a UV cutoff filter ($\lambda > 295$ nm) and was then focused onto a 90 ml cylindrical quartz reactor with a window (40 mm in diameter). The sample aliquots were intermittently withdrawn with a 1 ml syringe during UV irradiation and were filtered through a 0.45 mm PTFE filter (Millipore). The MB concentrations were monitored using a UV–visible spectrophotometer (Varian) at a wavelength of 665 nm.

The photocatalytic oxidation of gaseous CH_3CHO was determined in a closed circulated stainless steel reactor (volume 150 cm^3) that could be divided into two parts (upper and lower) by a control valve, similar to the setup described previously [26]. The gases used were CH_3CHO (300 ppmv in N_2) as a CH_3CHO standard; O_2 (99.9999%); and Ar (99.9999%) as a carrier gas. The concentrations of CH_3CHO and O_2 were 30–35 ppmv and 20%, respectively. Each photocatalyst was deposited onto a quartz plate sample holder with a 40 mm diameter. A 0.5 ml photocatalyst suspension of finely ground powder in distilled water was pipetted onto the center of the quartz-plate sample holder. After the dispersion of the suspension, the sample holder was dried at 100 °C for 3 h. The weight of each photocatalyst in the sample holder was approximately 5 mg. First, the mixed gas was passed through the empty upper reactor, and the concentration of CH_3CHO in the exit stream was monitored until it attained a constant value; the gas was then circulated in the reactor by the pump. Next, the circulated gas was passed through the lower reactor by controlling the valve so that the gas contacted the surface of the photocatalyst placed in the lower reactor. After adsorption equilibrium with the surface of the photocatalyst was established in the dark, the catalyst was illuminated with UV light. The distance between the sample and the lamp was 20 cm, and a cutoff filter ($\lambda < 295$ nm) was used. The removal of CH_3CHO was monitored using a gas chromatograph (GC, HP6890) that was equipped with a Porapak-Q column, a flame ionization detector (FID), a CO_2 methanizer (Ni catalyst), and a gas-sampling valve.

3. Results and discussion

3.1. Effects of surface modifications

The morphology and structure of the TiNT, TiNT–AT, TiNT–AT–AdP, and TiNT–AT–NaF were characterized by TEM (Fig. 1). Fig. 1a shows that the morphology of TiNT was poorly crystalline titanate nanotubes with outer diameters of approximately 70–80 nm. The formation of nanotubes by alkaline hydrothermal treatment has been previously described [6,9]. The titanate nanotubes could be formed by the slow dissolution of raw TiO_2 nanoparticles leading to epitaxial growth and exfoliation of layered nanosheets of titanate, followed by scrolling of the exfoliated nanosheets. The temperature of the alkaline hydrothermal treatment may significantly affect the morphology and crystallinity of the nanostructured titanates [12,27]. The TiNT consists of poorly crystalline titanate nanotubes, which is attributed to the relatively low temperature of the alkaline hydrothermal reaction. Moreover, the diameters of the TiNT nanotubes were larger than those of previously reported titanate nanotubes, which might be due to the stirring during the hydrothermal reaction. Bavykin et al. have reported that the intensification of the reaction rate has been achieved by stirring and that larger and more stable nanofibers were formed even at low temperature [21].

After being treated with 0.1 M HNO_3 at 80 °C for 24 h, the nanotubes were replaced by spherical nanoparticles, and elongated nanostructures were formed (Fig. 1b). Fig. 2a–c also show that the spherical-nanoparticle-embedded nanotubes and the elongated nanostructures coexisted. Titanate nanotubes have been previously reported to be transformed by acid treatment, and the rate of transformation depended on the concentration of the acid as well as on the temperature of the solution [19]. Therefore, the titanate nanotubes became predominantly elongated nanostructures through the phase-transition reaction under acidic conditions, whereas a minor portion of the titanate nanotubes slowly reacted with acid and formed spherical nanoparticles inside nanotubes. These morphological changes were related to the crystal phase transition. In Fig. 2d and e, the HR-TEM images of TiNT–AT show that the measured lattice distances of nanoparticles in nanotubes and elongated nanostructures were approximately 0.36 nm and 0.33 nm, which correspond to the (1 0 1) plane of anatase and the (1 1 0) plane of rutile, respectively [10]. The crystal structures of the spherical

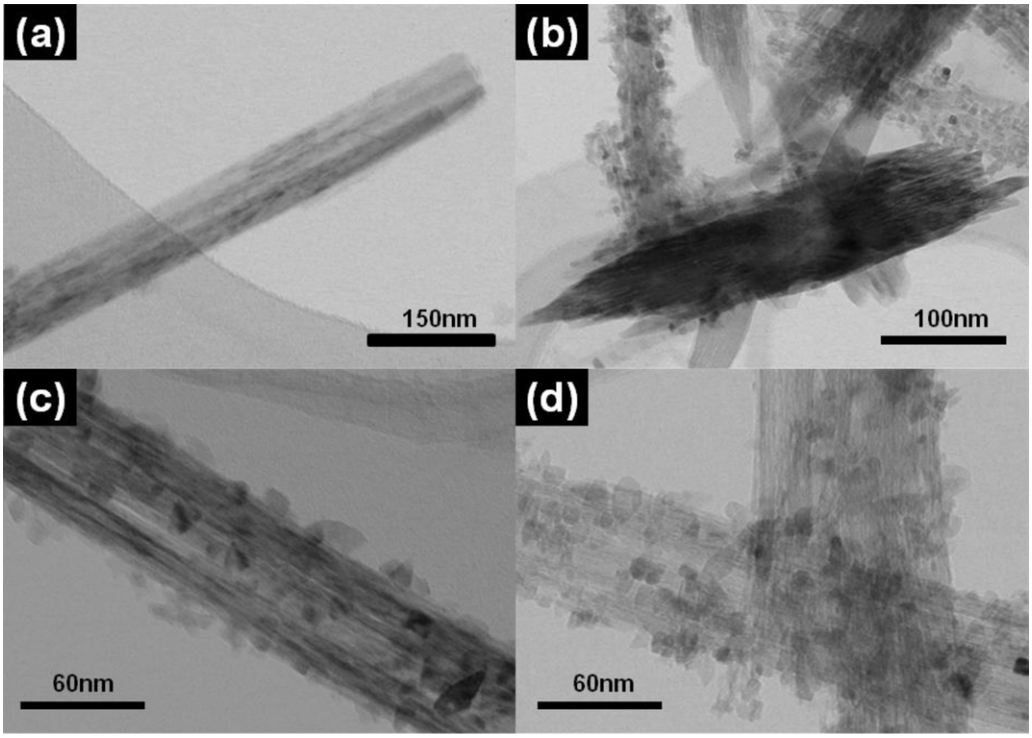

Fig. 1. TEM images of (a) TiNT, (b) TiNT–AT, (c)TiNT–AT–NaF, and (d) TiNT–AT–AdP.

nanoparticles and the elongated nanostructures thus corresponded to the anatase and rutile phases, respectively.

The morphology of the surface-modified TiNT–AT–AdP and TiNT–AT–NaF were significantly different from that of TiNT–AT, as shown in Fig. 1c and d, respectively. TiNT–AT–AdP and TiNT–AT–NaF comprised spherical nanoparticle decorated nanotubes. The formation of elongated nanostructures was inhibited through the surface modification with AdP and NaF, but the nanotube structures were undisturbed. This behavior might have been due to surface-adsorbed species preventing the transformation from titanate to the rutile phase of titania. The anatase-to-rutile transformation has been previously reported to be inhibited by surface modifications with compounds such as SiO_2 [28]. In addition, adsorbed phosphate has been reported to increase the crystallization temperature of metal oxides, such as Nb_2O_5, by decreasing their thermal mobility [29]. These surface modifications could also be responsible for the inhibition of rapid transition reactions from titanate to titania under acid treatment. Therefore, surface modification with AdP or NaF could be useful in maintaining the nanotubular structures under acid treatment.

Phase transitions were also observed in the XRD patterns (Fig. 3). The XRD pattern of TiNT indicated the presence of hydrogen titanate, which has a diffraction peak at 10° and corresponds to the interlayer spacing between the titanate sheets [9]. The XRD pattern of TiNT–AT showed relatively sharp peaks assigned to rutile and a few small peaks assigned to anatase. However, TiNT–AT–NaF and TiNT–AT–AdP showed only small, broad anatase XRD peaks. The difference in the XRD patterns confirmed the retarding effect of NaF and AdP on the titanate-to-rutile phase transition of titania.

Fig. 4 shows that the diffuse-reflectance UV–visible spectra of TiNT–AT, TiNT–AT–NaF, and TiNT–AT–AdP were red-shifted from that of TiNT. This result was consistent with previously reported results that showed that the band gaps of the titania phases, such as anatase and rutile, were smaller than those of the titanates [20]. The degree of shift was strongly related to the change in the crystalline phase of the samples. TiNT–AT with a rutile phase was more red-shifted than TiNT–AT–NaF and TiNT–AT–AdP. The band gaps were determined by the extrapolation of the linear portion of the plot of the Kubelka–Munk function against wavelength and were found to be 3.8, 3.4, 3.4, and 3.1 eV for TiNT, TiNT–AT–NaF, TiNT–AT–AdP, and TiNT–AT, respectively (Table 1).

Table 1 shows the results of the BET surface area measurements. The surface areas of untreated TiNT, TiNT–AT, TiNT–AT–NaF, and TiNT–AT–AdP were 126.2, 80.8, 151.3, and 188.2 m^2/g, respectively. The surface area was drastically reduced upon acid treatment, which was strongly related to the morphological change from hollow tubes to elongated nanostructures with spherical nanoparticles. However, the surface areas of the surface-modified samples were slightly increased after acid treatment, which might be due to the maintenance of the tube structures.

The existence of P and F atoms on the surface of samples was confirmed by XPS (Fig. 5). The P 2p signal for TiNT–AT–AdP was located at a binding energy of 133.6 eV, which corresponds to phosphate adsorbed on a TiO_2 surface [25]. However, the F 1s signal was not observed in TiNT–AT–NaF. This lack of signal might have been due to the fluoride ions in TiNT–AT–NaF being poorly adsorbed onto the TiNT–AT–NaF surface and being removed by washing and filtration after the acid treatment. During the acid treatment, fluoride ions are most likely largely adsorbed onto the surface of titanate. This absorption is strongly affected by the phase transition from titanate to titania because the complexation between the titanate surface and fluoride ions is favorable in acidic media.

Table 1
Physicochemical properties of the prepared samples.

	BET surface area (m^2/g)	BE (eV)[a]
TiNT	126.2	3.8
TiNT–AT	80.8	3.1
TiNT–AT–NaF	151.3	3.4
TiNT–AT–AdP	188.2	3.4

[a] Estimated using the plot of $[F(R_\infty)h\nu]^{0.5}$ vs. $h\nu$.

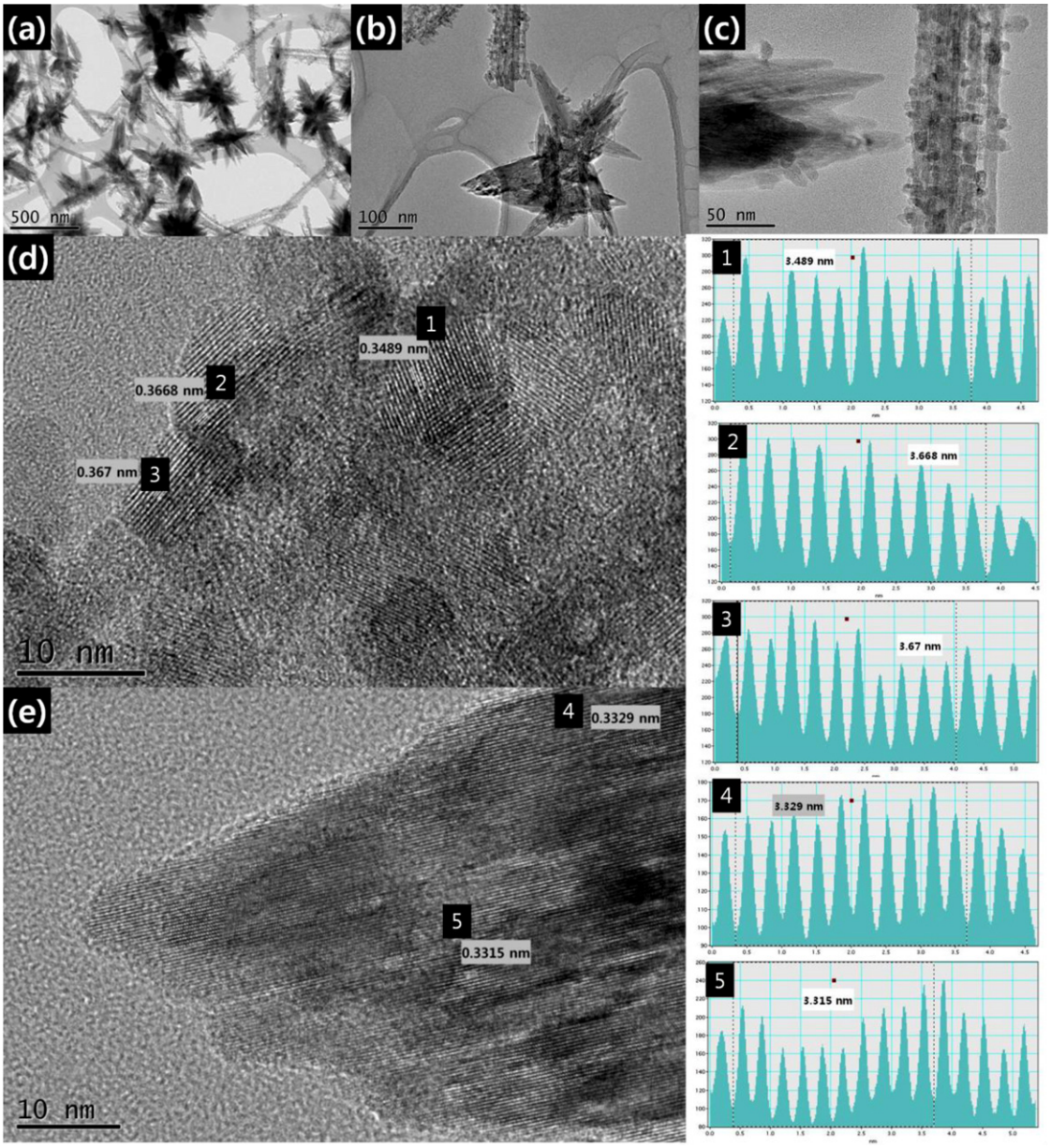

Fig. 2. HR-TEM images of TiNT–AT.

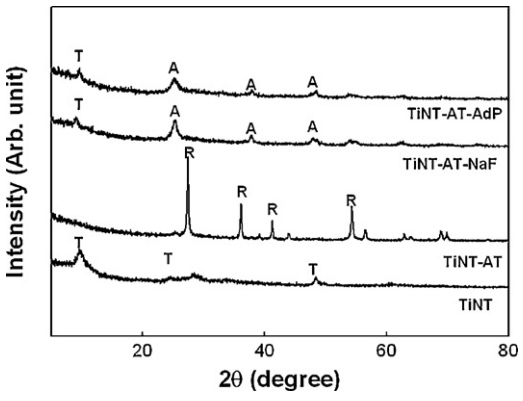

Fig. 3. XRD patterns of TiNT, TiNT–AT, TiNT–AT–NaF, and TiNT–AT–AdP.

On the basis of the previously discussed observations, we proposed the effects of surface modification by NaF or AdP addition in the acid-treatment reaction of TiNT shown in Fig. 6. During the acid treatment, hydrothermally prepared titanate nanotubes transformed into anatase-phase spherical nanoparticles and into rutile-phase elongated nanostructures as the nanotube structures were lost. However, in the presence of NaF or AdP, fluoride or phosphate ions adsorbed onto the surface of the titanate nanotubes stabilized the titanate phase during acid treatment. Therefore, the nanotubular structures were maintained, and anatase-phase spherical nanoparticles were only partly formed inside the nanotubes.

3.2. Photocatalytic activities

The adsorption and the photocatalytic degradation of MB by the nanomaterials of interest were investigated. Fig. 7 shows the change in the concentration of MB as a function of the UV

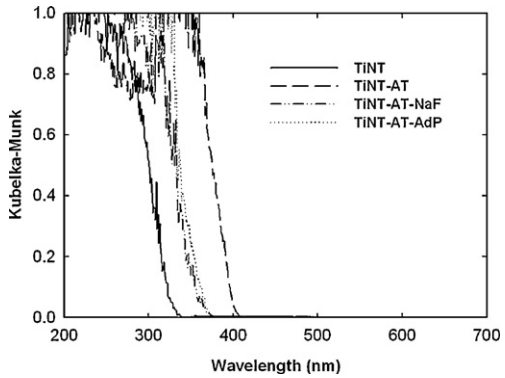

Fig. 4. DRS absorption spectra of TiNT, TiNT–AT, TiNT–AT–NaF, and TiNT–AT–AdP.

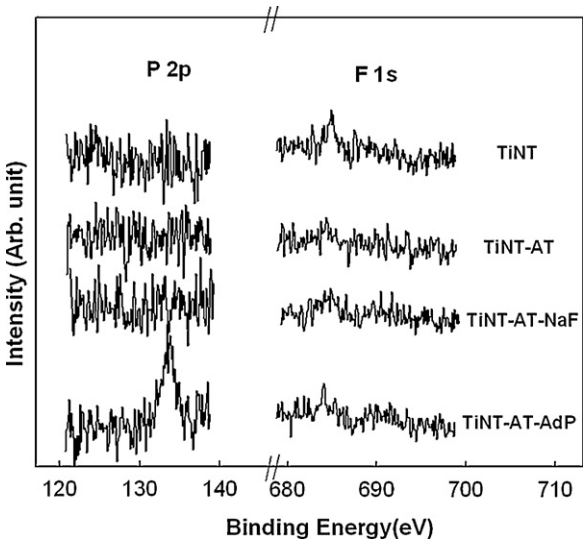

Fig. 5. P 2p and F 1s peaks in the XPS spectra of TiNT, TiNT–AT, TiNT–AT–NaF, and TiNT–AT–AdP.

irradiation time at pH 3 and pH 9. Because MB has a positive charge, the adsorption and degradation of MB are strongly affected by solution pH. In addition, the differences among the initial MB concentrations were caused by the adsorbed amount of MB (i.e., the MB concentration was measured using a UV–visible spectrophotometer after filtration, which was needed to remove the suspended particles, so the amount of MB adsorbed was not reflected in the absorption spectra). The initial adsorption of MB increased in the order TiNT–AT–NaF < TiNT–AT < TiNT–AT–AdP ≪ TiNT.

The adsorption of cationic MB was also strongly affected by the surface charge of the prepared samples. Fig. 8 shows the variation in the zeta potentials of TiNT, TiNT–AT, TiNT–AT–NaF, and TiNT–AT–AdP in water as a function of the pH. Upon acid treatment, the surface charge of TiNT was positively shifted. In addition, the pH of the zero point of charge (pH_{zpc}) of TiNT and TiNT–AT were measured to be pH 3.4 and pH 5.8, respectively. The negative charges on the surface were neutralized by the phase transition from titanate to anatase or rutile. However, the surface charges of TiNT–AT–NaF and TiNT–AT–AdP were significantly different. The surface charge of TiNT–AT–NaF was similar to that of TiNT–AT, whereas the pH_{zpc} of TiNT–AT–AdP was negatively shifted. Although both TiNT–AT–NaF and TiNT–AT–AdP were also neutralized by the phase transition from titanate to anatase, the surface of TiNT–AT–AdP contained phosphate groups (Fig. 6), and the surface charge of TiNT–AT–AdP was thus negatively shifted.

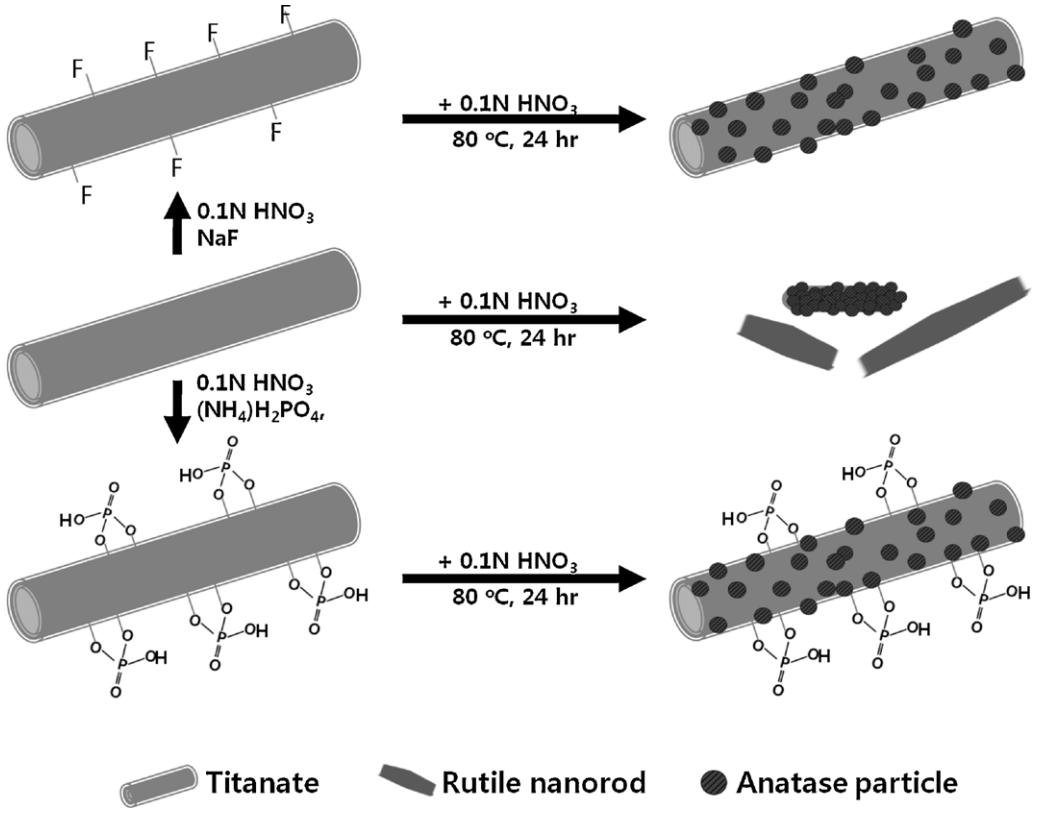

Fig. 6. Schematic of the effects of the surface modification by NaF or AdP in the acid-treatment reaction of TiNT.

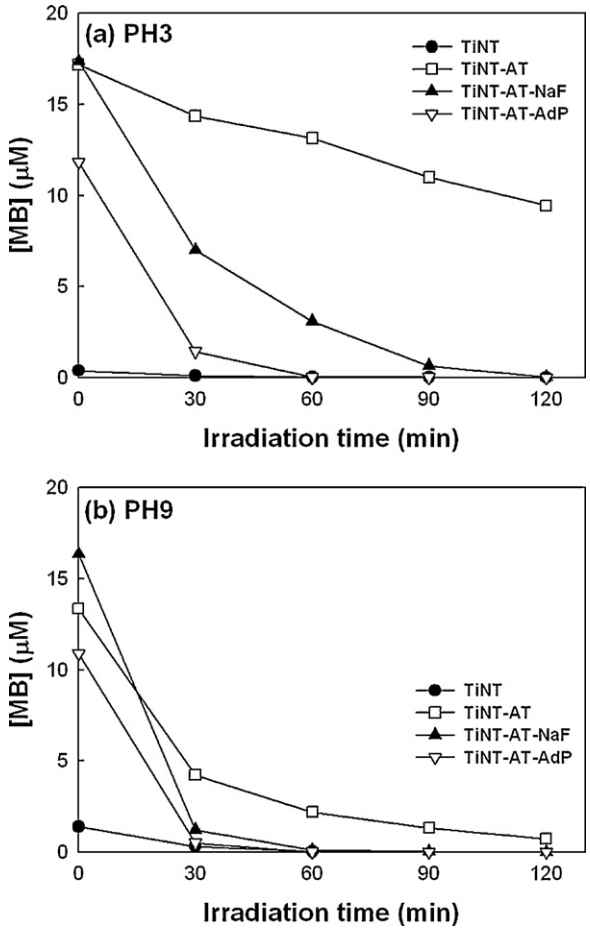

Fig. 7. Time-profiled MB degradation in UV-irradiated suspensions of TiNT, TiNT–AT, TiNT–AT–NaF, and TiNT–AT–AdP at (a) pH 3 and (b) pH 9. $[MB]_0 = 20\ \mu M$.

This shift may be responsible for the stronger adsorption of MB onto TiNT–AT–AdP than onto TiNT–AT–NaF.

On TiNT, MB was strongly adsorbed at both pH 3 and pH 9 because of the negatively charged surface. Although the change in MB concentration on UV-irradiated TiNT could not be determined, no color change in the test solution was observed (Figs. S1 and S2), which implied that the MB on the TiNT was not photocatalytically degraded. However, the TiNT–AT degraded the MB under UV irradiation, which appeared to result from the formation of the anatase and rutile phases of titania. Surface-modified TiNT–AT–NaF and TiNT–AT–AdP showed more efficient photocatalytic activity for MB degradation. This activity was likely due to the anatase phase having a photocatalytic activity greater than that of rutile, and the higher surface area of the nanotubular structures was more useful for the adsorption of MB.

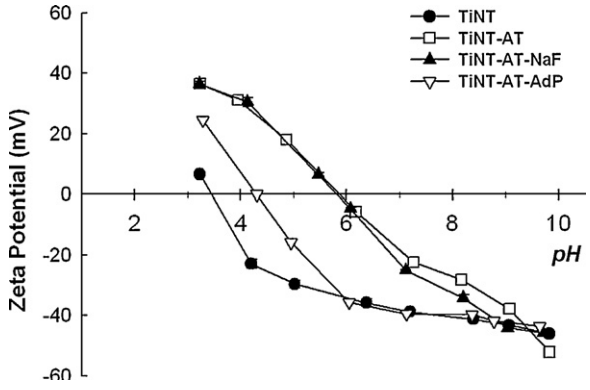

Fig. 8. Zeta potentials of TiNT, TiNT–AT, TiNT–AT–NaF, and TiNT–AT–AdP.

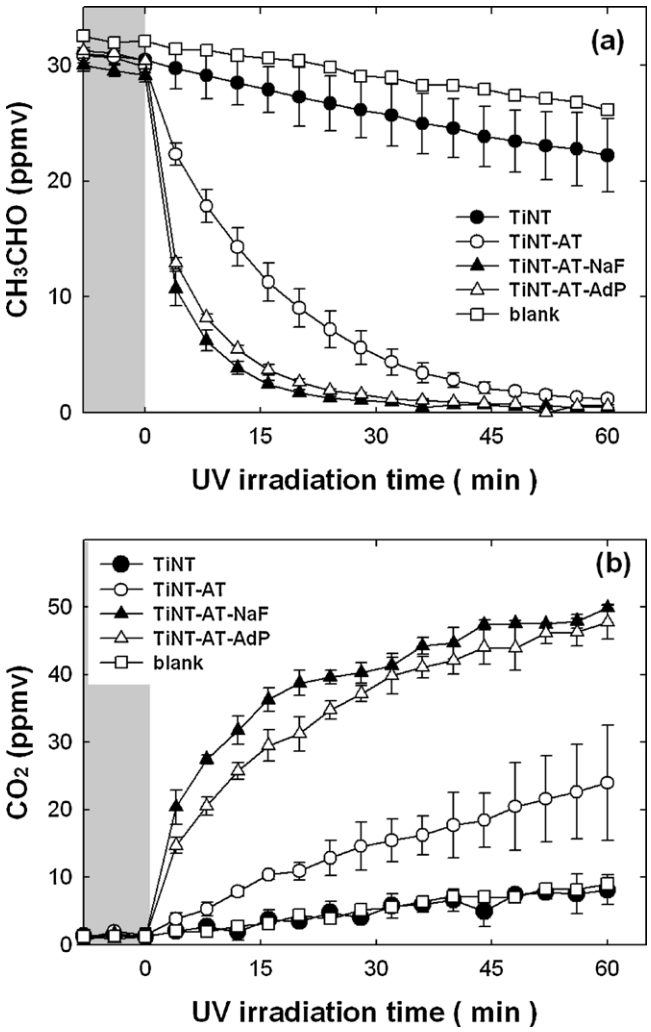

Fig. 9. Photocatalytic degradation of gaseous CH_3CHO on TiNT, TiNT–AT, TiNT–AT–NaF, and TiNT–AT–AdP.

The photocatalytic oxidation of gaseous CH_3CHO by the prepared materials was also investigated (Fig. 9), as was the simultaneous CO_2 production. The results were similar to those for the photocatalytic degradation of MB. The photocatalytic oxidation of gaseous CH_3CHO on TiNT was negligible. However, TiNT–AT exhibited efficient photocatalytic activity for gaseous CH_3CHO oxidation. Furthermore, surface-modified TiNT–AT–NaF and TiNT–AT–AdP showed increased photocatalytic activities for CH_3CHO oxidation and CO_2 production.

The photocatalytic activities of TiNT were negligible, whereas TiNT–AT was photocatalytically active. The phase transformation from titanate to titania with anatase may be responsible for the photocatalytic activities of TiNT–AT. However, during acid treatment, the nanotube structures were broken, and the BET surface area drastically decreased, which may explain why the photocatalytic activities decreased. When the surfaces were modified with NaF or AdP during the acid treatment, the nanotube structures were maintained, and the BET surface area was increased. As a result, both TiNT–AT–NaF and TiNT–AT–AdP showed efficient photocatalytic activities for MB degradation and CH_3CHO oxidation.

4. Conclusions

Hydrothermally prepared titanate nanotubes were transformed into titania upon acid treatment, which was accompanied by the destruction of the nanotube structures. However, these transitions and the destruction of the nanotube structures were inhibited by surface modification with NaF or AdP. The crystalline phases were also strongly affected by surface modification. After the acid treatment, the surface-modified TiNTs maintained their nanotube structures in the titanate phase, and spherical nanoparticles with an anatase phase were also formed on the nanotubes. In comparison, unmodified TiNTs transformed into rutile-phase elongated nanostructures and into anatase-phase spherical nanoparticles. Furthermore, the BET surface area was also increased by surface modification. Finally, the photocatalytic activities for MB degradation and gaseous CH_3CHO oxidation were strongly enhanced by the surface modifications, which was attributed to the anatase crystalline phase and the high surface area. Therefore, these surface modifications are useful methods to improve the photocatalytic activities of titanate nanotubes.

Acknowledgments

This work was supported by the DGIST R&D Program of the Ministry of Education, Science and Technology of Korea (11-NB-03). It was also supported by the Technology Innovation Program of the Ministry of Knowledge Economy of Korea (Industrial strategic technology development program, No. 10034046).

Appendix A. Supplementary data

Supplementary data associated with this article can be found, in the online version, at http://dx.doi.org/10.1016/j.apcatb.2012.05.008.

References

[1] X. Chen, S.S. Mao, Chemical Reviews 107 (2007) 2891–2959.
[2] H.H. Ou, C.H. Liao, Y.H. Liou, J.H. Hong, S.L. Lo, Environmental Science and Technology 42 (2008) 4507–4512.
[3] P. Hoyer, Langmuir 12 (1996) 1411–1413.
[4] D. Gong, C.A. Grimes, O.K. Varghese, W.C. Hu, R.S. Singh, Z. Chen, E.C. Dickey, Journal of Materials Research 16 (2001) 3331–3334.
[5] T. Kasuga, M. Hiramatsu, A. Hoson, T. Sekino, K. Niihara, Langmuir 14 (1998) 3160–3163.
[6] T. Kasuga, M. Hiramatsu, A. Hoson, T. Sekino, K. Niihara, Advanced Materials 11 (1999) 1307.
[7] A. Nakahira, T. Kubo, C. Numako, Inorganic Chemistry 49 (2010) 5845–5852.
[8] A. Nakahira, T. Kubo, C. Numako, ACS Applied Materials and Interfaces 2 (2010) 2611–2616.
[9] D.V. Bavykin, F.C. Walsh, Titanate and Titania Nanotubes: Synthesis, Properties and Applications, Royal Society of Chemistry, Cambridge, 2010.
[10] K. Kiatkittipong, C. Ye, J. Scott, R. Amal, Crystal Growth and Design 10 (2010) 3618–3625.
[11] C.C. Tsai, H. Teng, Langmuir 24 (2008) 3434–3438.
[12] K. Kiatkittipong, J. Scott, R. Amal, ACS Applied Materials and Interfaces 3 (2011) 3988–3996.
[13] J.G. Yu, G.H. Wang, B. Cheng, M.H. Zhou, Applied Catalysis B: Environmental 69 (2007) 171–180.
[14] J.G. Yu, H.G. Yu, B. Cheng, X.J. Zhao, Q.J. Zhang, Journal of Photochemistry and Photobiology A: Chemistry 182 (2006) 121–127.
[15] H.L. Kuo, C.Y. Kuo, C.H. Liu, J.H. Chao, C.H. Lin, Catalysis Letters 113 (2007) 7–12.
[16] C.H. Lin, J.H. Chao, C.H. Liu, J.C. Chang, F.C. Wang, Langmuir 24 (2008) 9907–9915.
[17] M.A. Khan, H.T. Jung, O.B. Yang, Journal of Physical Chemistry B 110 (2006) 6626–6630.
[18] Y.B. Mao, S.S. Wong, Journal of the American Chemical Society 128 (2006) 8217–8226.
[19] D.V. Bavykin, A.N. Kulak, V.V. Shvalagin, N.S. Andryushina, O.L. Stroyuk, Journal of Photochemistry and Photobiology A: Chemistry 218 (2011) 231–238.
[20] H.Y. Zhu, Y. Lan, X.P. Gao, S.P. Ringer, Z.F. Zheng, D.Y. Song, J.C. Zhao, Journal of the American Chemical Society 127 (2005) 6730–6736.
[21] D.V. Bavykin, A.N. Kulak, F.C. Walsh, Crystal Growth and Design 10 (2010) 4421–4427.
[22] M.S. Vohra, S. Kim, W. Choi, Journal of Photochemistry and Photobiology A: Chemistry 160 (2003) 55–60.
[23] H. Park, W. Choi, Journal of Physical Chemistry B 108 (2004) 4086–4093.
[24] J.S. Park, W. Choi, Langmuir 20 (2004) 11523–11527.
[25] J. Kim, W. Choi, Applied Catalysis B: Environmental 106 (2011) 39–45.
[26] S. Kim, S.K. Lim, Applied Catalysis B: Environmental 84 (2008) 16–20.
[27] S. Kim, M. Kim, S.H. Hwang, S.K. Lim, Journal of Industrial and Engineering Chemistry 18 (2012) 1141–1148.
[28] K. Okada, N. Yamamoto, Y. Kameshima, A. Yasumori, K.J.D. MacKenzie, Journal of the American Ceramic Society 84 (2001) 1591–1596.
[29] M.S.P. Francisco, W.S. Cardoso, Y. Gushikem, R. Landers, Y.V. Kholin, Langmuir 20 (2004) 8707–8714.